Article

Oxidation effects on short-term creep response in air of Commercially Pure Titanium (CP-2 Ti)

Michael Regev [1], Alberto Santoni [2] and Stefano Spigarelli [2,*]

[1] Mechanical Engineering Department, Braude College, P.O.Box 78, Karmiel 2161002, Israel
[2] Dipartimento di Ingegneria Industriale e Scienze Matematiche (DIISM), Università Politecnica delle Marche, via Brecce Bianche 60131, Ancona, Italy
* Correspondence: s.spigarelli@univpm.it

Abstract: The creep response of commercially pure titanium was investigated in air at 550, 600 and 650°C, to assess the effect of oxidation on the mechanical response. Experiments demonstrated that exposure at high temperature produced a marked reduction of the minimum creep rate under a given applied stress. Microhardness measurements showed that a hardened zone forms in proximity of the surface, due to oxygen penetration into metal. A simplified composite-model was then used to describe the creep response. In this model, the sample consisted of two zones, the hard case, enriched in oxygen, and the soft pure-titanium core, both creeping with similar strain rates. Calculation led to an estimation of the dependence of the minimum creep rate on stress and temperature for the hard high-oxygen zone. The simplified composite-model here presented gave an excellent description of experimental creep data for pure titanium tested in air and also provided a reliable picture of the effect of oxidation on complex Ti-alloys.

Keywords: creep; oxidation; titanium; constitutive equations

1. Introduction

The effect of oxidation on the creep response of titanium and its alloys is a subject that aroused keen interest among investigators, due to the importance of these materials for medium and high temperature applications. Detailed studies, such as [1], just to quote a single example, showed that oxidation reaction is very fast during the initial stage of the process and leads to the formation of oxide layers composed of TiO_2 structures. After this initial stage, the oxidation kinetics become very slow up to 650°C. In addition, a hard and brittle α-case rich in oxygen forms [2]. In castings, the α-case is the result of the reaction between liquid Ti metal and the mold wall, that leads to the early formation of TiO_2 and then of a hard solid-solution of oxygen into titanium on the surface of the part. The case is very brittle, and its cracking during straining causes early fracture of the sample [2]. This fact is of some relevance when creep tests on Ti and its alloy are carried out in air, since high temperature exposure also causes the penetration of oxygen into the alloy and the formation of the α-case [3]. Oxygen exposure results in a reduction of the minimum creep rate [3,4], although an opposite behavior was once observed [5], by testing a single experimental condition. In this context, the analysis of the creep response in air of commercially pure titanium remains an interesting subject to be dealt with.

This study is part of a wider research aimed at clarifying the effect of friction stir welding (FSW) [6] on the creep response in air of commercially pure Titanium. To properly identify the effects of the extensive microstructural changes introduced by FSW on the creep response, the independent effect of oxidation should be preliminary quantified. This part of the study aimed at investigating this phenomenon, trying to quantify the effect of oxygen enrichment on the minimum creep rate dependence on stress and temperature.

Preprints (www.preprints.org) | NOT PEER-REVIEWED | Posted: 8 June 2023 doi:10.20944/preprints202306.0624.v1

2. Materials and Methods

The material investigated in the present study was commercially pure Ti – grade 2 (CT-Ti Gr.2, UTS of 500 MPa) in form of a plate 3 mm thick. Dog-bone creep samples with the geometry illustrated in [6] (3 mm x 3 mm square section, 25 mm gauge length) were creep-tested in constant load machines at 550, 600 and 650°C. Two types of experiments were carried out: constant load experiments (CLEs) and variable load experiments (VLEs). In most of the CLEs, the samples were loaded after soaking for 0.5 h at the testing temperature, and the load was maintained until interruption of the tests, well in tertiary stage but before fracture. Two CLE samples were annealed at the test temperature (650°C) for 70 h before loading. In VLEs, the sample was loaded after soaking, but the initial load was maintained until the minimum creep rate was reached and then increased until a new value of the minimum creep rate was attained.

To maintain a homogeneous heating profile in the furnace, the test temperature was measured using four thermocouples. Elongation was continuously measured using a linear variable displacement transducer (LVDT). All creep experiments were carried out in air.

Crept samples were mechanically ground and polished with a colloidal suspension and etched by Kroll's reagent (100 mL H_2O + 2 mL HF + 4 mL HNO_3), and then observed by a Leica DMi8 (Leica Microsystems, Wetzlar, Germany) optical microscope.

Microhardness measurements were carried out on sample heads, under a 25 g load, i.e., in unstrained portions of the specimen, to evaluate the hardening effect of oxygen and its penetration.

3. Results

3.1. Creep response

Figure 1 plots the strain rate *vs* strain curves for CLEs and VLEs; the stress values are the nominal ones, calculated with reference to the initial area of the transversal sample section. The creep curves exhibited the usual conventional three-stage shape, with a well-defined primary region, a minimum creep rate range and a prolonged tertiary stage. An interesting feature is that after load-changes in VLEs, the minimum creep rates are usually well below those recorded under similar loads in CLEs. This phenomenon is well apparent at 600°C and at 650°C, see, for example, the VLE at the highest temperature, where the strain rate under 40 MPa (nominal; the true stress value was 42.9 MPa) is much lower than that measured in a CLE under the same nominal stress. The same behavior is illustrated in Figure 1d, which shows the CLE tests carried out under 20 and 40 MPa (nominal) after 0.5 and 70 h soaking at testing temperature. The samples annealed for 70 h exhibit substantially lower values of the strain rate at a given stress.

Table 1 summarizes the experimental values of the minimum creep rate ($\dot{\varepsilon}_m$). Figure 2 plots the minimum creep rate as a function of the true stress (σ), i.e., the stress corresponding at the strain in which the minimum in creep rate was measured. Figure 2a does not discriminate between the data obtained by CLEs or VLEs and seems to suggest that the usual power law

$$\dot{\varepsilon}_m \propto \sigma^n \qquad (1)$$

is substantially obeyed. A major point is that the stress exponent n, quite unusually, increases with temperature, from 4.6 at 550°C to 5.8 at 650°C. A clearer picture of the material response, on the other hand, can be obtained by differentiating the symbols of the experimental data, according to the duration of high-temperature exposure they experienced when the considered minimum creep rate was recorded (Figures 2 b-d).

Preprints (www.preprints.org) | NOT PEER-REVIEWED | Posted: 8 June 2023 doi:10.20944/preprints202306.0624.v1

Table 1. Summary of results of the experimental tests.

test	Temperature [°C]	Stress, nominal [MPa]	Minimum strain rate [s^{-1}]
VLE10	650	6	$1.9x10^{-9}$
		15	$1.8x10^{-7}$
		40	$8.0x10^{-5}$
CLE14	650	12	$5.2x10^{-7}$
CLE13*	650	20	$3.0x10^{-6}$
CLE01	650	20	$6.0x10^{-6}$
CLE05	650	32	$6.2x10^{-5}$
CLE02	650	40	$2.2x10^{-4}$
CLE08*	650	40	$1.4x10^{-4}$
CLE06	650	45	$3.6x10^{-4}$
VLE12	600	10	$1.6x10^{-8}$
		25	$2.5x10^{-6}$
		35	$1.6x10^{-5}$
VLE11	600	15	$2.3x10^{-7}$
		44	$7.3x10^{-5}$
CLE20	600	40	$4.0x10^{-5}$
CLE07	600	41	$4.9x10^{-5}$
CLE04	600	60	$2.6x10^{-4}$
CLE03	600	70	$5.0x10^{-4}$
VLE19	550	15	$2.3x10^{-8}$
		82	$4.4x10^{-5}$
CLE18	550	20	$1.3x10^{-7}$
CLE20	550	30	$1.0x10^{-6}$
CLE17	550	40	$3.7x10^{-6}$
CLE16	550	60	$2.1x10^{-5}$
CLE15	550	100	$3.0x10^{-4}$

* The sample was loaded after 70h at the testing temperature

Figure 2 clearly suggests that indeed the experimental data roughly align on parallel straight lines, which shift toward lower strain rates when time of exposure increases. Thus, both Figures 1 and 2 demonstrate that high-temperature exposure results in a substantial hardening of the sample. This effect can hardly be explained in terms of microstructural mechanisms in this pure metal unless the effect of oxidation in considered. Thus, a more detailed and quantitative analysis of the hardening effect of oxidation was required.

Preprints (www.preprints.org) | NOT PEER-REVIEWED | Posted: 8 June 2023 doi:10.20944/preprints202306.0624.v1

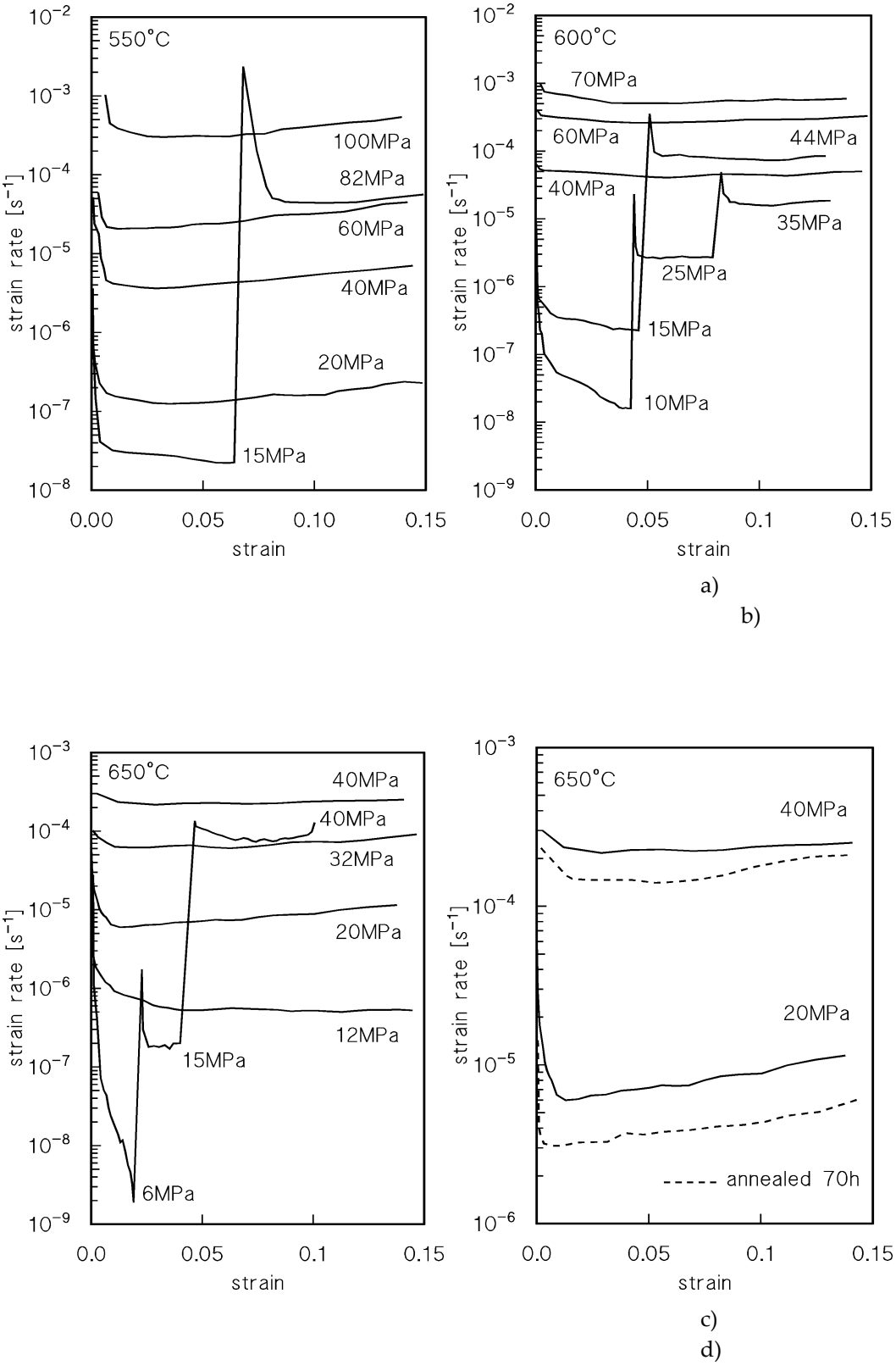

Figure 1. Strain rate vs strain creep curves: a) 550°C; b) 600°C; c) 650°C; d) 650°C, effect of annealing for 70h before loading at the testing temperature.

Preprints (www.preprints.org) | NOT PEER-REVIEWED | Posted: 8 June 2023 doi:10.20944/preprints202306.0624.v1

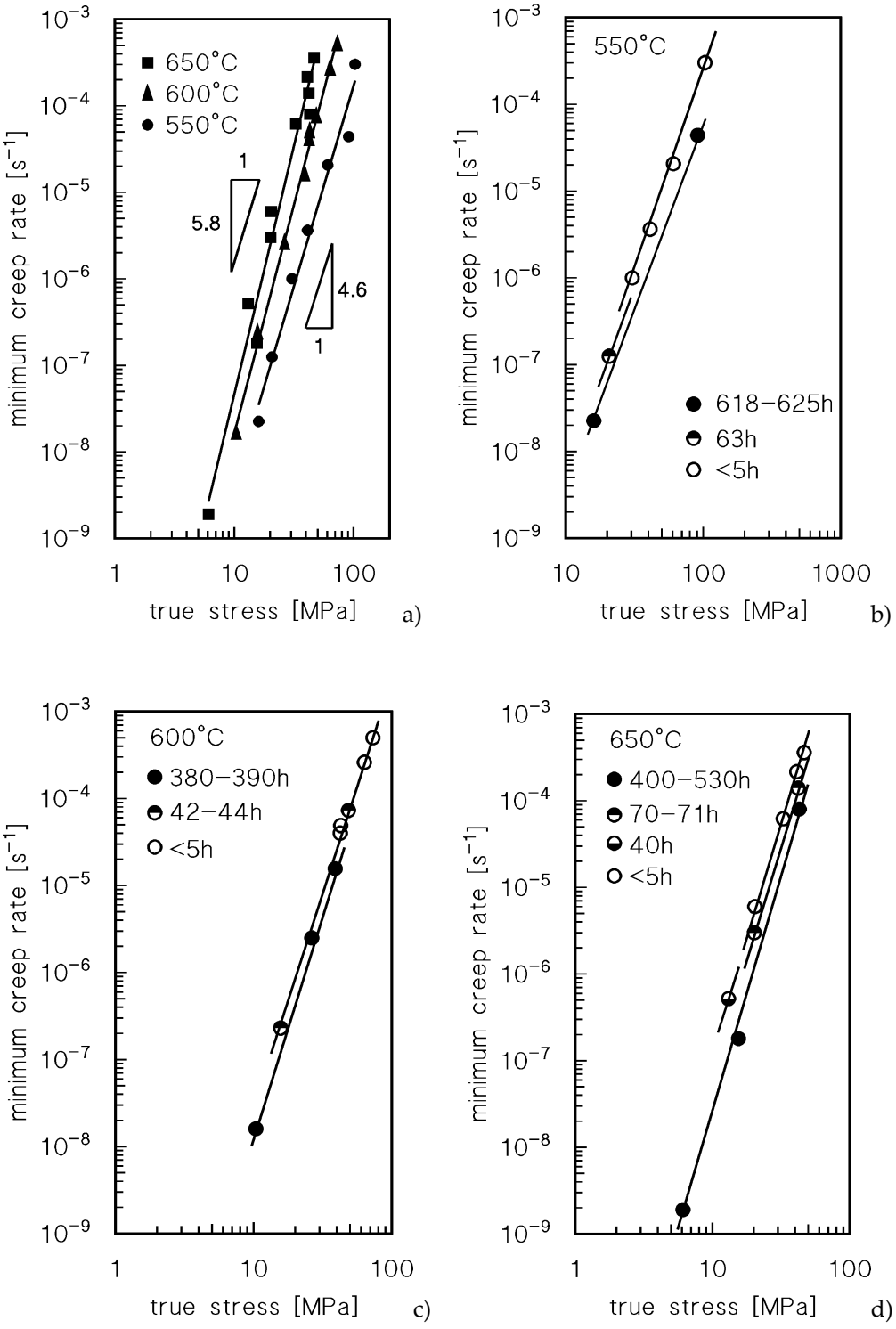

Figure 2. Minimum strain rate as a function of true stress: a) all experiments; b) 550°C; c) 600°C; d) 650°C. In b), c) and d) symbols are differentiated according to the duration of high temperature exposure in correspondence of the minimum creep rate.

Preprints (www.preprints.org) | NOT PEER-REVIEWED | Posted: 8 June 2023 doi:10.20944/preprints202306.0624.v1

3.2. Oxidation and hardening effect: microhardness profiles

Figure 3a shows an example of the microhardness measurements on the heads of the samples that experienced a long exposure at high temperature. As expected, the highest was the temperature and the longest was the duration of exposure, the highest was the hardness of the surface and the thicker was the hardened zone. Formation of a hard and brittle oxide surface layer at 650°C for the longest times of exposure, on the other hand, is easily noticeable in Figure 3a. This oxide layer was much thinner or even unnoticeable for lower temperatures and/or shorter times of exposure.

The hardening effect illustrated in Figure 3 is fully consistent with similar evidence in the literature, which demonstrates that this behavior is due to oxygen diffusion in Ti (see, for example, [7, 8]). Thus, a correct estimation of oxygen penetration in the material becomes an interesting point to be analyzed.

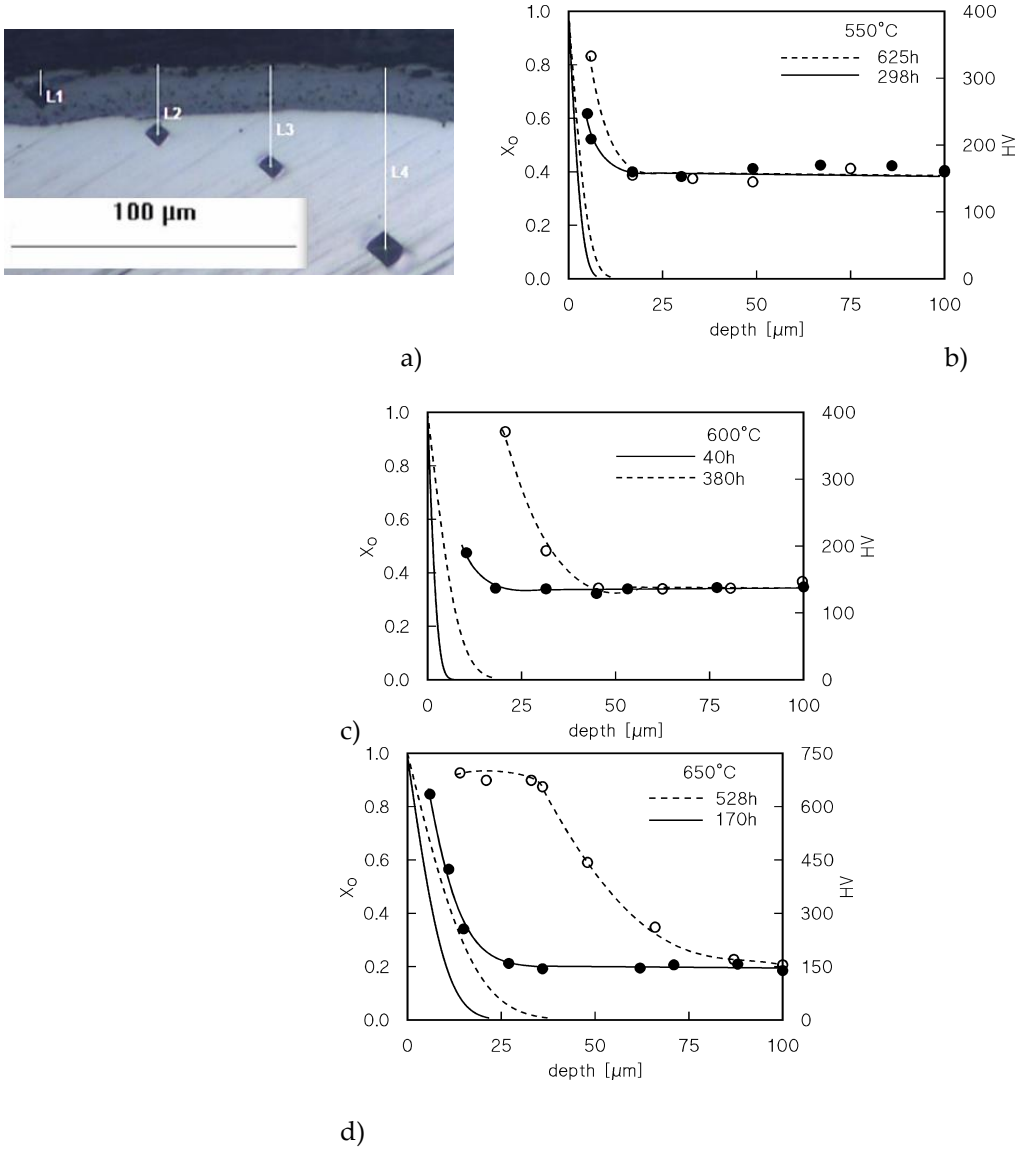

Figure 3. a) Microhardness measurements in the VLE sample tested at 650°C for 625 h; b-d) microhardness (circles) and calculated profile of oxygen (*Xo* parameter, curves) for the longest tests at 550°C (b), 600°C (c) and 650°C (d). Circles represent the hardness values.

Preprints (www.preprints.org) | NOT PEER-REVIEWED | Posted: 8 June 2023 doi:10.20944/preprints202306.0624.v1

The simplest model for oxygen penetration [9] is the solution of Fick's second law in semi-infinite material, which assumes a constant concentration at the surface and a constant diffusion coefficient, i.e.

$$X_O = \frac{C_x - C_0}{C_s - C_0} = 1 - erf\left[\frac{x}{2\sqrt{Dt}}\right] \quad (2)$$

where C_0 is the initial oxygen concentration in the metal, C_s is the surface concentration, C_x is the concentration at the distance x from the surface, t is time and D is the diffusion coefficient of oxygen in Ti, i.e.

$$D = D_0 exp\left(-\frac{Q}{RT}\right) \quad (3)$$

where D_0=2x10^{-7} s^{-1} and Q=169 kJ mol^{-1} [10]. Figure 3, which also plots the X_O variation with the distance from the surface, shows that the increase is microhardness is notable even where the enrichment in oxygen is so low to be unnoticeable.

Figure 4a re-plots the hardness profile for the sample-head that experienced the longest permanence at 650°C (528 h). The Figure also includes the typical value of the hardness in correspondence of the oxide surface layer, omitted in Figure 3d.

Preprints (www.preprints.org) | NOT PEER-REVIEWED | Posted: 8 June 2023 doi:10.20944/preprints202306.0624.v1

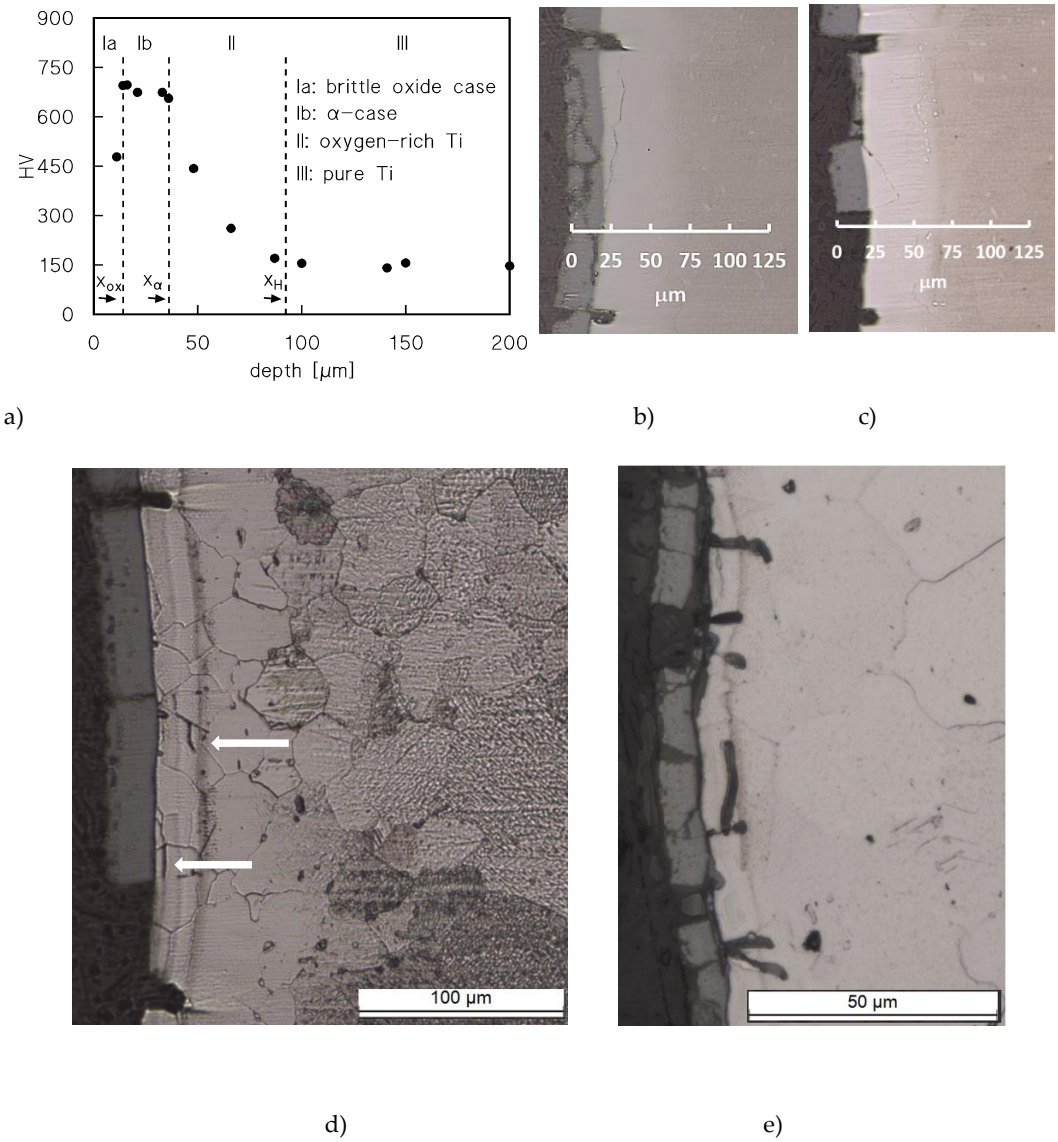

a) b) c)

d) e)

Figure 4. a) Microhardness profile on the head of the sample that experienced a prolonged (528 h, VLE10) holding at high temperature; b-c) gauge length, cracking of the oxide layer of zone Ib; both large cracks of length ≈(x_{ox} + x_α), perpendicular to the surface, and longitudinal fine cracks which propagate under the oxide layer, can be easily observed. The oxide layer is heavily cracked and, in many locations, detached from the underlying oxygen-rich zone; d) gauge length, microstructure after etching, with vertical fissures occasionally appearing in different locations of the oxygen-rich layer, near the surface (white arrows); e) unetched gauge length after creep at 650°C, CLE13, overall exposure duration 171 h.

The Figure shows the existence of four different zones: i. the oxide surface layer (Ia), which cracks even under the HV indenter, and, possibly for this reason, exhibits a relatively low HV value; ii. an intermediate zone (Ib) of almost constant and very high (roughly 700 HV) microhardness; these HV values attest a brittle nature [11,12], hardly capable of tolerating any notable deformation [2]; iii. a zone of decreasing hardness (II); iv: the un-oxidized core of the sample. For the sake of clarity and simplicity, we will assume in the following paragraphs that zone-Ib corresponds to what is usually called "α-case" in Ti and Ti-alloys.

Preprints (www.preprints.org) | NOT PEER-REVIEWED | Posted: 8 June 2023 doi:10.20944/preprints202306.0624.v1

Figures 4b-d show extensive cracking in the oxide layer, which is detached from the underlying oxygen-rich zones. Many wide cracks, perpendicular to the loading direction, pass through zones Ia and Ib. Finer cracks also develop in zone Ib, but propagate along directions parallel to the surface. Figures 4d shows the different metallographic contrast between the base metal and the oxygen-rich zone (the bright area) after etching. The bright area is indeed much thicker (100 μm) than the estimate of the penetration of oxygen as provided by Eqns.2-3 (≈40 μm). The situation is similar in the sample tested under 20 MPa after a 70 h-soaking at 650°C (Figure 4e). Again, the oxide layer is heavily damaged, and cracks propagate for roughly 10 μm in the oxygen-rich zone.

4. Discussion

4.1 Strengthening role of oxygen-rich layers

The main issue to properly address the role of the different layers is the identification of the strengthening contribution of zones Ia, Ib and II. Early cracking of the undeformable surface layers during creep straining should significantly reduce their strengthening role. In particular, the oxide layer largely detaches from the substrate during creep (Figure 4), and for this reason its strengthening contribution can be thought to be negligible. On the other hand, cracking in the scarcely deformable layer-Ib during early creep deformation, also illustrated in Figure 4b-e, interrupts the local material continuity, undermining its load-bearing capacity [2]. Thus, also zone-Ib should give a negligible contribution to the creep response in correspondence of the minimum creep rate. This analysis is fully consistent with Rosen and Rottem findings [3]. These authors removed from few oxidized samples what they identified as the "α-case", i.e., presumably, what corresponded mostly to zone-Ib in Figure 4. The identification of the Rosen-Rotten "α-case" with zone-Ib is justifiable, since they were fully aware that the microhardness descended toward the original value of the unoxidized Ti-6Al-4V (zone-II in Figure 4a) beyond the depth of their "α-case". Its removal from the exposed specimen did not significantly change the minimum creep rate, since $\dot{\varepsilon}_m$ remained roughly 1/3 of that measured in absence of oxidation, as in samples which maintained their α-case. This fact proved that the real strengthening effect was played by the oxygen-reach zones below the α-case.

Vaché and Monceau [9] proposed a model equation for the decrease in hardness with distance from the surface of oxidized material in the form:

$$X_{HV} = \frac{HV_x - HV_0}{HV_{max} - HV_0} = \sqrt{1 - erf\left[\frac{x}{2\sqrt{Dt}}\right]} \qquad (4)$$

where HV_0 is hardness of the metal with initial oxygen concentration, HV_{max} is the maximum hardness, HV_x is the hardness at the distance x from the point where HV_{max} is measured, usually the surface. Equation 4 implies a parabolic relationship between microhardness and oxygen concentration, so that a constant HV corresponds to a constant oxygen content. On the other hand, based on the above reasoning, both the oxide layer (thickness x_{ox}) and the α-case (thickness x_α) do not contribute to creep strengthening. Thus, Eqn.4 could be tentatively used to quantify the hardness variation with depth in zone-II, under the layers of depth (x_{ox}+ x_α). Figure 5 plots the variation of hardness with depth according to Equation 4, with HV_{max}=700 HV and HV_0=150 HV. The correlation between the curves and the experimental profiles is reasonably good, so Equation 4 can be used to estimate the depth of the hardened oxygen-rich zone-II which causes a significant reduction of the creep rate. The limit for this layer was here tentatively quantified as the x value corresponding to X_{HV}=0.01.

Preprints (www.preprints.org) | NOT PEER-REVIEWED | Posted: 8 June 2023 doi:10.20944/preprints202306.0624.v1

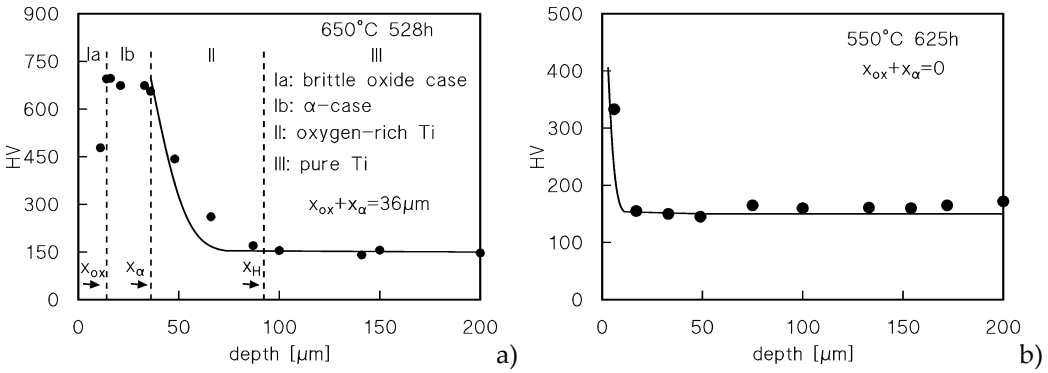

Figure 5. Hardness variation with depth for representative samples; HV_{max}=700 HV; HV_0=150 HV.

4.2. Constitutive equation for CP-Ti (no or minor effects of oxidation)

A very good description of the creep response of a dataset of pure Ti samples [14] was recently provided by an equation whose derivation was illustrated in detail in [15, 16]. This equation assumes the form:

$$\dot{\varepsilon}_m = A\frac{D_{0L}Gb}{kT}\left(\frac{\sigma}{G}\right)^3 exp\left(\frac{\sigma b^3}{kT}\right) exp\left\{-\frac{Q_L}{RT}\left[1-\left(\frac{\sigma}{R_{max}}\right)^2\right]\right\}, \quad (5)$$

where D_{0L}=1x10^{-8} m^{2}s^{-1} and Q_L=193 kJ mol^{-1} describe the self-diffusion mechanism in low-purity Ti through Eqn. 3 [17], G is the shear modulus, b is the length of the Burgers vector (2.95x10^{-10} m), T is the absolute temperature, k is the Boltzmann constant, R is the gas constant, A=40 [15]. The R_{max} parameter was tentatively obtained as follows [15]:

$$R_{max} = 1.5UTS\frac{G_T}{G_{RT}}, \quad (6)$$

where G_{RT} and G_T were the shear moduli at room temperature and at testing T, respectively. Figure 6 plots the minimum creep rate *vs* stress curves calculated by Eqn. 5 with A=40 and R_{max} from Eqn.6 [15], compared with the data from [14] and the results of the present study from CLEs of short durations, where oxidation can be reasonably assumed to have minor effects. In case of the samples tested in [14], oxidation could be in first instance neglected, due to the substantially larger size of the samples (5 mm in diameter; this point will be further discussed in the following). The Figure demonstrates that the constitutive equation, in this form, strongly underestimates the creep rate in the high stress regime. Reconsidering the quantification of the R_{max} term is thus needed; a much better description was indeed obtained with

$$R_{max} = 2.8\ \mathrm{UTS}_T, \quad (7)$$

where UTS_T is the tensile strength at testing temperature, and A=50. This simple modification led to a much better description of the creep response of CP-2 Ti in the intermediate and high strain rate regimes (solid lines in Figure 5).

The next step was the study of the effect of oxidation on the value of the minimum creep rate for longer test duration.

Preprints (www.preprints.org) | NOT PEER-REVIEWED | Posted: 8 June 2023 doi:10.20944/preprints202306.0624.v1

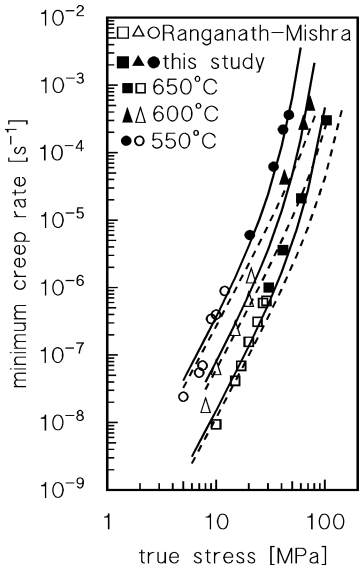

Figure 6. Experimental data for pure Ti from [14] (round samples 5mm in diameter) and from present study (CLE, very short test duration), and calculated curves from Eqn.6; broken lines: A=40, R_{max} from Eqn.6, with UTS=500 MPa; solid lines: A=50, R_{max} from Eqn.7, with UTS_T= 105, 75 and 55 MPa at 550, 600 and 650°C (obtained from data for annealed CP-2 Ti in [18]).

4.2. Quantification of the effect of oxidation on creep response

The evidence on the marked differences in creep rate between CLEs and VLEs provided in the previous section, demonstrates that oxidation results in an increase in microhardness and in a reduction in creep rate under a given stress. Pure Ti, in proximity of the surface, significantly enriches in oxygen as time of exposure increases. Thus, a "hard zone" (II in Figure 4), not homogeneous in composition, encloses a core of pure Ti. It is obvious that such a complex material can be hardly modelled unless a strong simplification of its structure is applied. In the present study, the real material has been very simply modelled as presented in Figure 7. Following this approach, based on the well-known composite-material-model (CMM), the soft core of the sample (unmodified pure Ti) is surrounded by a hard layer of oxygen-rich titanium of homogeneous composition and properties. The latter assumption is thus the major departure from the real situation, since in the crept samples the oxygen content progressively reduces as the distance from the surface increases.

Figure 7. Composite-material-model (CMM) of the oxidized creep sample. A soft interior zone (pure Ti, light grey) is surrounded by an external hard zone (oxygen-rich Ti, dark grey) of depth x_H. a) section, side 3 mm; b) gauge length (tensile axis is horizontal). For the sake of simplicity, the hard zone is homogeneous in oxygen content and properties, an obvious deviation from the real case.

The depth of the hard surface layer, x_H, can be approximatively estimated by Eqn.4, in correspondence of the minimum creep rate. The volume fraction of the hard zone, the surface layer rich in oxygen, can be thus expressed as

Preprints (www.preprints.org) | NOT PEER-REVIEWED | Posted: 8 June 2023 doi:10.20944/preprints202306.0624.v1

$$f_H = 1 - f_S = 1 - \left(\frac{l-2x_H}{l}\right)^2 \quad (8)$$

where l is the length of side of the square sample section, here taken= 3 mm, thus neglecting the effect of elongation, and f_S is the volume fraction of the unmodified Ti soft zone.

In the CMM of Figure 7, both the hard and soft zones deform in parallel with the same creep rate, under different local stresses (σ_H and σ_S respectively). As a result, load is transferred from the soft to the hard portions of the sample, giving,

$$\sigma = f_H\sigma_H + (1 - f_H)\sigma_S \quad (9)$$

To make a proper use of Eqn.9, the constitutive equation correlating stress, temperature and strain rate for the hard zone should be available. This is a major – and practically unsolvable- problem, due to the complete lack of information about the creep response of O-rich titanium. Nevertheless, one can reasonably assume that the model-material for the hard zone creeps according to the classical phenomenological equation:

$$\dot{\varepsilon}_m = A_H{\sigma_H}^n exp\left(-\frac{Q_H}{RT}\right) \quad (10)$$

where A_H and n, in this simplified approach, are constant, and Q_H is an apparent activation energy. For the sake of simplicity, it will be here supposed that also Q_H is stress and temperature independent. In case of the VLE at 650°C, the 3 data points correspond to times of exposure of 400, 513 and 528 h, while for the VLE at 550°C the two values of the minimum creep rate were obtained after 618 and 632 h. Equation 4 was then used to estimate x_H for X_{HV}=0.01 after 450 h at 650°C, and 620 h at 550°C, which gave f_H and f_S. For a given strain rate, σ_S is obtained directly from Eqns. (5) and (7). The model parameters A_H, n and Q_H were thus tentatively estimated by a fitting procedure of the VLE data at 650°C and 550°C. A good fit of the VLE data at 650 and 550°C was obtained by taking n=10, A_H=1x10^8 s^{-1} MPa^{-10} and Q_H=620 kJ mol^{-1}. Once estimated the parameters in Eqn.10, the CMM can be easily used to obtain the model curves at 550, 600 and 650°C for different exposure durations. Figure 8 plots a direct comparison between experimental data and model curves. The curves for exposures shorter than 5 h were calculated by assuming that oxidation did not occur. In general term, the accuracy of the model is more than acceptable.

Figure 8d reports the experimental data from [14]. The authors did not specify if a protective atmosphere was used, which led one to suppose that testing was performed in air. Unfortunately, no information on the time of exposure in correspondence with the minimum creep rate can be deduced from the source, since the creep curves reported in [14], one CLE (interrupted after 50 h, estimated strain rate =5x10^{-8} s^{-1}) and one VLE (load change after 70 h, estimated strain rate =2x10^{-8} s^{-1}), indeed applied to a composite. Nevertheless, one can reasonably assume that a similar testing scheme was followed when investigating unreinforced Ti, that is, for minimum creep rates in the range from 2x10^{-8} to 5x10^{-8} s^{-1}, the time corresponding $\dot{\varepsilon}_m$ should range between 50 and 100 h. If 70 h for the time of exposure is used to estimate x_H and the relevant f_H volume fraction in a sample 5 mm in diameter, as used in [14], the model curve reported in Figure 8d is obtained. The description of the low-stress experimental data is indeed quite accurate.

Preprints (www.preprints.org) | NOT PEER-REVIEWED | Posted: 8 June 2023 doi:10.20944/preprints202306.0624.v1

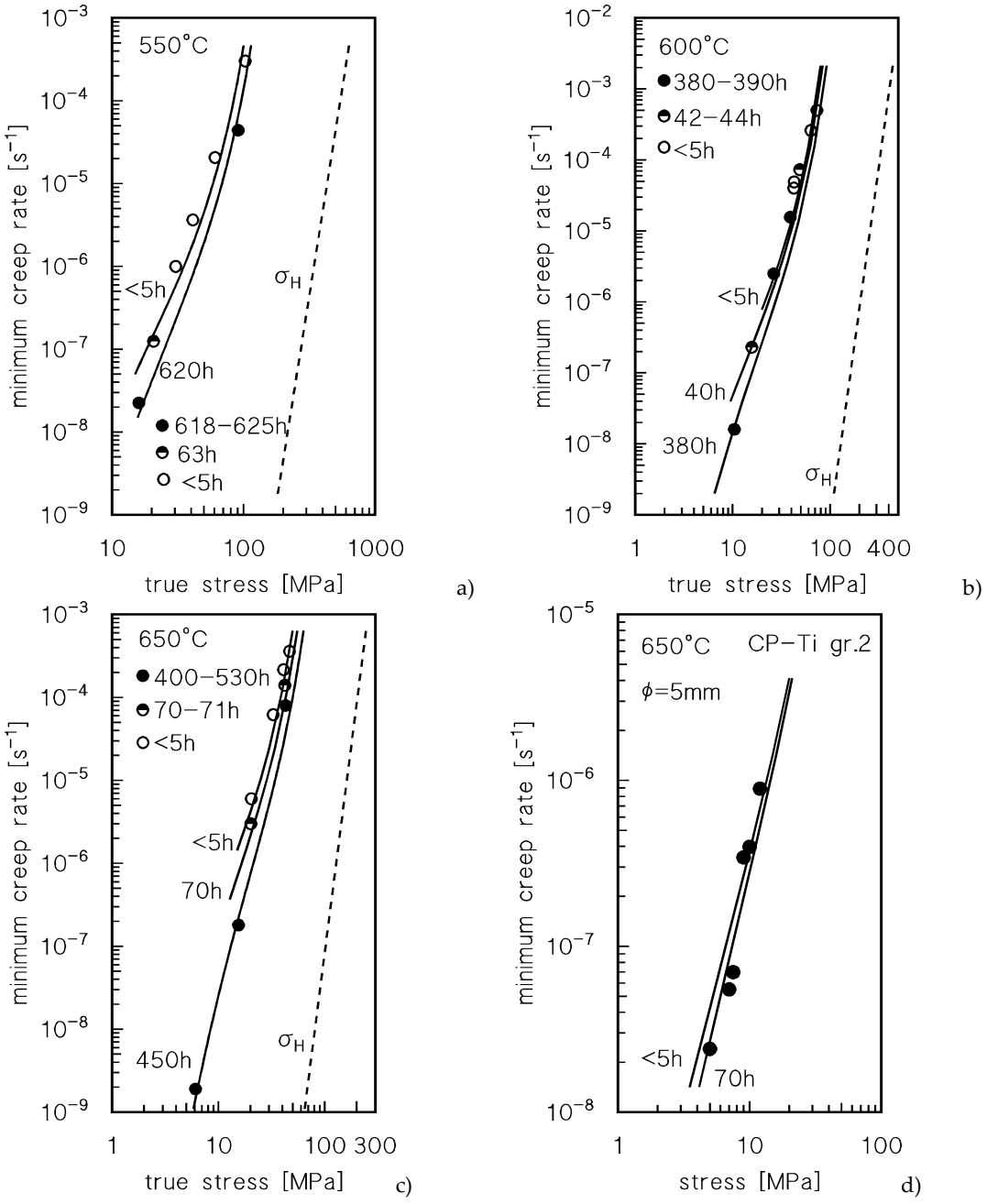

Figure 8. Comparison between model curves and experimental data (a, b, c, 3mmx3mm sample; d, round sample 5mm in diameter): a) 650°C, model curves calculated for exposure durations of 0, 63 and 620 h; b) 600°C, model curves calculated for exposure durations of 0, 40 and 380 h; c) 650°C model curves calculated for exposure durations of 0, 70 and 450 h; d) 650°C, data from [14], model curves calculated for exposure durations of 0 and 70 h for a sample 5 mm in diameter (Φ).

4.2. Critical assessment of the model

The CMM in the form presented here was based on a highly simplified picture of the real situation, and, for this reason, it did not have the ambition to provide a physically-based description of creep of oxygen-rich Ti (a task otherwise impossible to be fulfilled, due to the already mentioned lack of experimental data). Thus, another obvious question could be raised: is the quantification of the creep strength of the hard zone, shown in Figure 8, reasonable?

To answer this question, we must firstly address the problem of the possible strengthening mechanisms operating in the oxygen-rich zones. Even a relatively moderate content

Preprints (www.preprints.org) | NOT PEER-REVIEWED | Posted: 8 June 2023 doi:10.20944/preprints202306.0624.v1

of oxygen (0.8%) increases the UTS of pure Ti well above 1000 MPa, with a hardness just below 400 HV [19,20]. According to Figures 3-5, the oxygen-rich zone-II exhibits experimental microhardness values in the range between 200 and 600 HV. For reference purpose, Ti-6Al-4V alloy [15,16] usually exhibits an UTS close to 1000 MPa. This fact implies that oxygen-rich pure-Ti is assimilable, in terms of mechanical properties, to more complex industrial alloys. The source of this remarkable strength is usually attributed to solid solution hardening [11], namely, it may depend on a strong interaction between screw dislocation cores and oxygen atoms. In addition, a recent study provided evidence that even small additions (0.15%) of oxygen cause the formation of ordered precipitates with a Ti_6O-type structure [12]. These ordered precipitates were observed also in CP-Ti grade 2 [12]. Thus, the oxygen-rich layer is indeed a very complex material, where solid solution hardening and possibly particle-dislocation interaction play a significant role in enhancing strength at room and high temperatures. In the present study, the complex oxygen-rich zone-II was "replaced" by a model-material with a homogeneous O content, well above 0.15%, and with different x_H thicknesses. Due to the high oxygen content, solid solution should be surely operative there. If also the ordered precipitates play any hardening role, which is realistic, the use of the phenomenological Eqn.10 for the model-material should indeed result in high values of the apparent stress exponent and activation energy (n and Q_H) [16], exactly as those here tentatively estimated.

Let one suppose that the creep properties of the oxygen-rich layers in Ti-6Al-4V are reasonably close to those here calculated for pure Ti. Rosen and Rottem investigated the effect of a pre-oxidation of 3 h in air at 900°C on the creep response at 400°C of the Ti-6Al-4V [3]. Pre-oxidation produced an "α-case" ≈140 μm thick. The samples were tested by VLE, but creep deformation did not exceed a total strain of 1%, which suggests a possible overestimation of the minimum creep rate under the lowest stresses - see, for example, the shape of the strain-rate *vs* strain curves in [15,16]. The Rosen and Rottem creep data for the alloy annealed at 900°C in vacuum were thus compared with those published by Whittaker et al. [21], Figure 9a. The Figure also plots the model curve for Ti-6Al-4V, calculated, as above, by Eqn.5, with the same values of the various parameters used in [15] (D_{0L}=1.4x10^{-3} m^{2}s^{-1}, Q_L=303 kJ mol^{-1} [17], R_{max}≈1150 MPa) and A=50. The model curve as obvious does not consider the effects of oxidation. The Figure shows that the agreement between the model curve and the data from [21] is more than tolerable. In addition, it confirms that the values of the low-stress minimum creep rate calculated by Rosen and Rottem by VLEs should be treated cautiously, although they still represent an invaluable source of information on the behavior of the alloy in oxidized and non-oxidized states (Figure 9b). The minimum creep rate values for exposed material are significantly lower than those for the material annealed in vacuum.

Now, let us assume, as suggested in the previous section and following Rosen and Rottem reasoning, that the α-case, i.e. the more superficial O-rich layer, Ib, does not significantly affect the minimum creep rate values of the exposed alloy, in our view because, as the strain accumulates, cracks develop in this zone. No information was provided on the oxide scale, so it will be here neglected. The cracks do not usually penetrate beyond the α-case in creep tests of relatively short duration [22]. This thick layer could be thus even removed, without significantly influencing the creep response. The thickness of the oxygen-rich zone II after 3 h at 900°C, given by Eqn.4 for X_H=0.01, is x_H=44 μm. The CMM (Eqns.8-10) provides the broken curve in Figure 9b for the exposed material, to be compared with the model curve for the alloy annealed in vacuum (no oxidation, same curve in Figure 9a). Further oxidation at the testing temperature, 400°C, could be reasonably neglected. If one considers the predictable overestimation of the creep rates under the lower stresses in [3], the agreement between model curves and experiments is notably accurate. We have thus a direct confirmation of the adequacy of this simplified approach to estimate the effect of oxidation for Ti alloys.

Preprints (www.preprints.org) | NOT PEER-REVIEWED | Posted: 8 June 2023 doi:10.20944/preprints202306.0624.v1

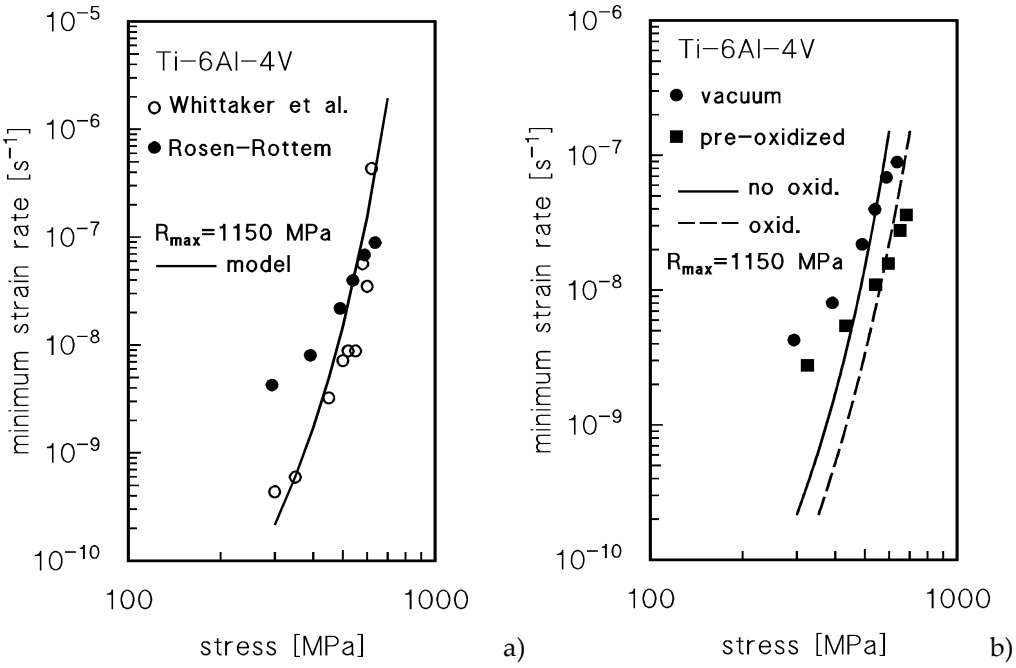

Figure 9. a) Minimum creep rate 400°C for the Ti-6Al-4V alloy annealed at 900°C-3h in vacuum [3], and for a similar alloy with bimodal α+β microstructure [21]. The model curve (no effects of oxidation) was calculated by eqn.5 with D_{0L}=1.4x10^{-3} m^{2}s^{-1}, Q_L=303 kJ mol^{-1} [17], R_{max}≈700 MPa and A=50. b) Rosen and Rottem data [3] from VLE at 400°C for the Ti-6Al-4V annealed at 900°C for 3h in vacuum or in air. The curves represent the behavior of un-oxidized and oxidized alloys (see text for details).

5. Conclusions

The creep response in air of CP-2 titanium was investigated at temperatures of 550, 600 and 650°C. Experimental data demonstrated that high-temperature exposure resulted in a marked decrease of the creep rate, suggesting a hardening role of the oxygen-rich layer formed during tests. The growth of the hard superficial layer was thus modelled as a function of temperature and time of exposure. The creep sample was modelled as a composite formed by an inner soft core (pure titanium) and a hard outer zone rich in oxygen and homogeneous in composition and properties. Fitting of two variable-load experiments at 550 and 650°C were used to quantify the creep response of the hard-zone. The resulting composite model, although based on an overly simplified description of the real structure, was able to provide an excellent description of the material response in all the investigated range of temperatures and test durations. The model also provides a quite reliable description of the creep response of more complex Ti-alloys, such as the Ti-6Al-4V.

Author Contributions: Conceptualization, M.Regev and S.Spigarelli.; methodology, S.Spigarelli; validation, M.Regev and S.Spigarelli; formal analysis, M.Regev, A.Santoni and S.Spigarelli; investigation, M.Regev, A.Santoni and S.Spigarelli; resources, M.Regev; data curation, S.Spigarelli; writing—original draft preparation, S.Spigarelli ; writing—review and editing, M.Regev and S.Spigarelli; visualization, M.Regev and S.Spigarelli; supervision, S.Spigarelli; project administration, M.Regev; funding acquisition, M.Regev. All authors have read and agreed to the published version of the manuscript.

Funding: This research project is partially funded by Braude College, Karmiel, Israel.

Data Availability Statement: The data presented in this study are available on request from the corresponding author.

Acknowledgments: The assistance of N. Navot with welding the material is highly appreciated

 doi:10.20944/preprints202306.0624.v1

Conflicts of Interest: The authors declare no conflict of interest.

References

1. Gemelli, E.; Camargo, N.H.A. Oxidation kinetics of commercially pure titanium. Revista Matéria, 2007, 12, 525-531, http://www.materia.coppe.ufrj.br/sarra/artigos/artigo1091
2. Chan, K.S.; Koike, M.; Johnson, B.W.; Okabe, T. Modeling of Alpha-Case Formation and Its Effects on the Mechanical Properties of Titanium Alloy Casting, Metall. Mater. Trans. 2008, 39A, 171-180. https://doi.org/10.1007/s11661-007-9406-0.
3. Rosen, A.; Rottem, A. The Effect of High Temperature Exposure on the Creep Resistance of Ti-6AI-4V Alloy. Mater, Sci. Eng. **1976**, *22*, 23-29.
4. Poquillon; D.; Parrens, C.; Pugliara, A.; Perrais, M., Malard, B. Oxidation of Ti–6Al–4V alloy between 450 and 600°C. Evolution of microstructure and mechanical properties. *MATEC Web of Conferences* **2020**, *321*, 06009. https://doi.org/10.1051/matecconf/202032106009.
5. Reis, D.A.P.; Piorino, F.; Barboza, M.J.R.; Nono, M.C.A.; Silva, C.R.M. Influence of the oxidation in creep of Ti-6Al-4V alloy. *Acta Microscopica* **2003**, *12*, 219-220.
6. Regev, M.; Almoznino, B.; Spigarelli, S. A Study of the Metallurgical and Mechanical Properties of Friction-Stir-Welded Pure Titanium. *Metals* **2023**, *13*, 524. https://doi.org/10.3390/met13030524
7. Kalienko, M; Volkov, A.; Leder, M.; Zhelnina A. Study of oxygen content in titanium alloys after exposure at elevated temperature, *MATEC Web of Conferences* **2020**, *321*, 11068, https://doi.org/10.1051/matecconf/202032111068.
8. Gardner, H. M.; Gopon, P.; Magazzeni, C.M.; Radecka, A.; Fox, K.; Rugg; D.; Wade, J.; Armstrong, D.E.J.; Moody, M.P.; Bagot, P.A.J. Quantifying the efect of oxygen on micro-mechanical properties of a near-alpha titanium alloy. *J. Mater. Res.* **2021**, *36*, 2529-2544, https://doi.org/10.1557/s43578-020-00006-3.
9. Vaché, N.; Monceau, D. Oxygen Diffusion Modeling in Titanium Alloys: New Elements on the Analysis of Microhardness Profiles. *Oxidation of Metals* **2020**, *93*, 215-227. https://doi.org/10.1007/s11085-020-09956-9.
10. Bregolin, F.L.; Behar, M.; Dyment, F. Diffusion study of 18O implanted into α-Ti using the nuclear resonance technique, *Appl. Phys*. **2007**, *A 86*, 481–484. https://doi.org/10.1007/s00339-006-3782-y.
11. Yu, Q.; Qi, L.; Tsuru, T.; Traylor, R.; Rugg, D.; Morris, J.W.J.; Asta, M.; Chrzan, D.C.; Minor; A.M. Origin of dramatic oxygen solute strengthening effect in titanium. *Science* **2016**, *347*, 635-639.
12. Poulain, R.; Delannoy, S.; Guillot, I.; Amann, F.; Guillou, R.; Lartigue-Korinek, S.; Thiaudière, D.; Béchade, J.-L.; Clouet, E.; Prima, F. First experimental evidence of oxygen ordering in dilute titanium–oxygen alloys, *Materials Research Letters* **2022**, *10*, 481-487. https://doi.org/10.1080/21663831.2022.2057202
13. Magazzeni, C.M.; Gardner, H.M.; Howe, I.; Gopon, P.; Waite, J.C.; Rugg, D.; Armstrong, D.E.J.; Wilkinson, A.J. Nanoindentation in multi-modal map combinations: a correlative approach to local mechanical property assessment. *J. Mater. Res*. **2021**, *36*, 2235-2250. https://doi.org/10.1557/s43578-020-00035-y.
14. Ranganath,S.; Mishra, R.S. Steady state creep behaviour of particulate-reinforced titanium matrix composites, *Acta Mater*. **1996**, *44* , 927-935. https://doi.org/10.1016/1359-6454(95)00242-1.
15. Spigarelli, S.; Paoletti, C.; Cabibbo, M.; Cerri, E.; Santecchia, E. On the creep performance of the Ti-6Al-4V alloy processed by additive manufacturing, *Additive Manufacturing* **2022**, *49*, 102520. https://doi.org/10.1016/j.addma.2021.102520.
16. Spigarelli, S.; Paoletti, C.; Cerri, E.; Santecchia, Cabibbo, M. Creep response of Ti–6Al–4V alloy produced by additive manufacturing: Effect of annealing at 1050°C. *Mater, Sci. Eng*. **2022**, *A860*, 144278. https://doi.org/10.1016/j.msea.2022.144278.
17. Perez, R.A.; Nakajima, H.; Dyment, F. Diffusion in α-Ti and Zr, *Mater. Trans*. **2003**, *44*, 2–13. https://doi.org/10.2320/matertrans.44.2.
18. Shahmir, H.; Pereira, P.H.R.; Huang, Y.; Langdon, T.G. Mechanical properties and microstructural evolution of nanocrystalline titanium at elevated temperatures, *Mater. Sci. Eng*. **2016**, *A669*, 358-366. http://dx.doi.org/10.1016/j.msea.2016.05.105.
19. Bieler, T.R; Trevino, R.M.; Zeng, L. Alloys: Titanium, *Encyclopedia of Condensed Matter Physics, Reference Module in Materials Science and Materials Engineer*ing **2005**, 65-76. https://doi.org/10.1016/B0-12-369401-9/00536-2.
20. Luo, S.D.; Song, T.; Lu, S.L.; Liu, B.; Tian, J.; Qian, M. High oxygen-content titanium and titanium alloys made from powder. *J. All. Comp*. **2020**, *836*, 155526. https://doi.org/10.1016/j.jallcom.2020.155526.

 doi:10.20944/preprints202306.0624.v1

21. Whittaker, M.T.; Harrison, W.J.; Lancaster, R.J.; Williams, S. An analysis of modern creep lifing methodologies in the titanium alloy Ti6-4, *Mater. Sci. Eng*. **2013**, *A577*, 114-119. http://dx.doi.org/10.1016/j.msea.2013.03.030.
22. Evans, R.W.; Hull, R.J.; Wilshire, B. The effects of alpha-case formation on the creep fracture propertied of the high-temperature titanium alloy IMI834, J.Mater.Proc.Techn. 1996, 56, 492-501. https://doi.org/10.1016/0924-0136(96)85109-0.